MARS PATHFINDER CRUISE STAGE/ ENTRY VEHICLE SEPARATION DYNAMICS

Chia-Yen Peng and Kemeth S. Smith

Spacecraft Structures and Dynamics Group
Mechanical Engineering Section
Mechanical Systems Engineering and Research Division
Jet Propulsion Laboratory
California Institute of Technology
Pasadena, CA 91109, USA

ABSTRACT

Prior to atmospheric entry, Mars Pathfinder flight system will separate its entry vehicle from its cruise stage, and establish the entry conditions for a passive and unconventional entry, descent, and landing approach. This paper summarizes a separation dynamics analysis conducted to demonstrate that the cruise separation system design is viable and ensure that adequate design margins exist with the effects from parameter uncertainty included.

Enhanced by the Monte Carlo technique, the separation analysis predicts the statistical bounds of separation velocity, entry attitude error, and a subset of critical clearances with 990/. confidence. These statistical bounds are used to assess the performance of the current cruise separation hardware design under worst case conditions

The results indicate that the current design satisfies the separation requirements, provided drag forces in the cable cutter barrel are less than approximately 18 N per cutter.

NOMENCLATURE

α	total entry attitude error, i.e., angle of attack of entry vehicle
θ_{NAV}	entry attitude error due to navigation error
θ_{AIM}	entry attitude error due to pointing error
θ_{SEP}	entry attitude error due to cruise separation
μ	post-separation nutation of entry vehicle
v	wobble angle of entry vehicle
H_{EV}	post-separation angular momentum vector of entry vehicle

1. 1NTRODUCTION

Mars Pathfinder is a Discovery program missicm designed to deliver a lander, camera and instrument-laden rover to the surface of Mars, demonstrating a new and unconventional atmospheric entry and landing approach. The spacecraft will be launched on December 2, 1996, from Cape Canaveral, Fla., and spend seven months cruising to Mars. On July 4, 1997, Mars Pathfinder will land on an ancient flood basin known as Ares. Mars Pathfinder is part of a new generation of low-cost spacecraft designed by the Jet Propulsion Laboratory to explore planets and other celestial bodies of the solar system [1].

Twenty-four hours before Mars arrival, the flight system will turn approximately 7 degrees to its entry attitude. Thirty minutes prior to atmospheric entry, the spacecraft will then jettison its cruise stage, as shown in Figure 1, and dive directly into the Martian atmosphere, braking with an a eroshell, parachute and small solid retrorockets before landing with the aid of huge, multi-lobed airbags.

A successful cruise stage/entry vehicle separation is very critical to the mission. Since it is very difficult and expensive to test this separation event, an extensive dynamic analysis has been undertaken to predict the separation velocity, clearance loss, and entry vehicle angle of attack at atmospheric entry.

2. ANGLE OF ATTACK OF ENTRY VEHICLE

The angle of attack of the entry vehicle on atmospheric entry is defined as the angle between the aerodynamic symmetry (z) axis of the entry vehicle and its velocity vector relative to the atmosphere of Mars. The current

analysis uses the following equation to compute the maximum entry vehicle angle of attack a, i.e.,

$$\alpha = \sqrt{\theta_{NAV}^2 + \theta_{AIM}^2 + \theta_{SEP}^2} + \mu + \nu , \qquad (1)$$

where α is the angle of attack of the entry vehicle; θ_{NAV} is the angle between the ideal and actual target vector; θ_{AIM} is the angle between the actual target vector and the spacecraft pre-separation angular momentum vectors; θ_{SEP} is the angle between the pre-separation angular momentum vector of spacecraft and the post-separation angular momentum vector of entry vehicle; μ is the post-separation nutation of entry vehicle; and v is the (wobble) angle between the principal axis of entry vehicle and the aerodynamic symmetry (z) axis of entry vehicle.

To ensure the aerodynamic stability of the Mars Pathfinder entry vehicle, the allowable entry vehicle attitude error at atmospheric entry is only 7°. As a result, the major challenge of the current separation analysis is to account for all the dominant factors affecting entry error:

- Pre-separation spin and nutation;
- Mass properties of cruise stage and entry vehicle;
- Propellant fill level and migration between tanks;
- Separation torque induced by spring mismatch;
- Separation torque imparted by cable cutter drag.

3. MONTE CARLO SIMULATION

An important aspect of separation analyses is the uncertainty of model parameters (mass properties, initial conditions, spring parameters, geometric data, etc.). In order to account for the randomness associated with such uncertainty, the Monte Carlo technique was incorporated in the cruise separation analysis. Monte Carlo simulation provides a unified framework for the quantitative analysis of model uncertainty and assessment of associated risk, and in the formulation of trade-off studies relative to design parameters [2]. The use of high-speed workstations has made Monte Carlo simulation more practical as a design and verification tool.

The ingredients of the Monte Carlo simulation of the Mars Pathfinder cruise stage/entry vehicle separation dynamics are:

- Dynamic model to simulate cruise separation;
- Random selection of model parameters;
- Statistical bounds of simulation outputs.

4. DYNAMIC MODEL

In order to simulate the cruise separation event, a three dimensional 12-DOF rigid body dynamic model was developed using the ADAMS (Automatic Dynamic Analysis of Mechanical Systems) program [3]. This mode] has been parametrized and used as a template to generate actual ADAMS input files. The model parameters in the template will be randomly selected for each run. The model parameters to be selected are:

- Propellant fill level and mass properties;
- Mass properties of cruise stage and entry vehicle;
- Separation spring parameters;
- Cable drag at two cutter locations;
- Pre-separation spacecraft spin and nutation.

5. RANDOM MODEL PARAMETER SELECTION

A MATLAB program was written to randomly generate 100 sets of model parameters prior to the Monte Carlo simulation. The random variables (or constants) used to generate these sets are listed in Table 1. The generation procedure is described in the following sections.

5.1 Propellant Fill Level & properties

The propellant in four fuel tank is a significant portion of the total fight system mass. The amount of propellant remaining at the time of separation is dependent on injection accuracy and other unknowns. For this analysis, the total propellant at separation was distributed uniformly from O to 85 kg. The propellant mass properties are functions of fill level and propellant center of mass (cm.) errors due to temperature imbalance and bladder asymmetry. The steps to select the propellant mass properties are:

1. Randomly select total propellant mass of 4 tanks, based on M_p_tot, Table 1;
2. Compute corresponding fill level, based on

Figure 1. ADAMS animation of Mars Pathfinder Cruise Separation

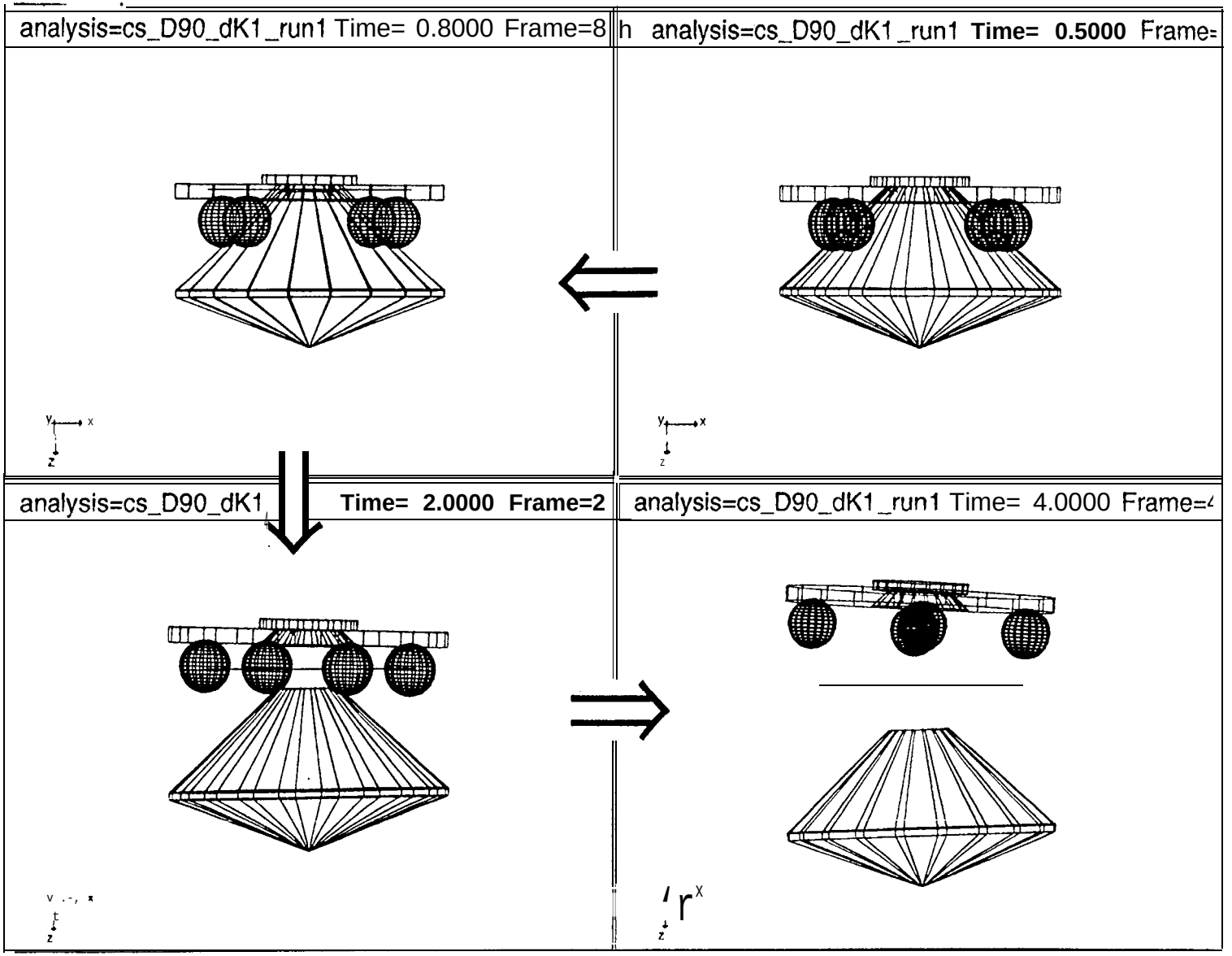

Table 1. Variables Used for Random Selection of Model Parameters

Variable Name	Min./ Mean	Max./ 3Sigma	Dist.	Units	Description
M_p_tot	*o*	85	uniform	kg	Total propellant mass of four tanks
M_p_max	25		constant	kg	Propellant mass per tank at maximum fill level
f_max	64.9		constant	%	Maximum fill level of propellant tanks
Ltc	1.045		constant	m	Nominal radius of propellant tank center
Ztc	0.35		constant	m	Nominal height of propellant tank center
Dtc	o	*0.005*	normal	m	Propellant tank misalignment
z_p	*		constant	m	Nominal height of propellant C.M. above tank center
dR_p "	*o*	*	normal	m	Propellant C.M. offset, x-y plane, per tank
dZ_p	*o*	*	normal	m	Propellant C.M. offset, z axis, per tank
M_m	*o*	*0.9*	uniform	kg	Fuel migration between tanks, per axis
M_sv	665	821	uniform	kg	Mass of full system (dry)
M_v	*0.7*	*0.74*	uniform	no unit	Mass ratio of entry vehicle vs. full system (dry)
J3m_sv	0.58	0.62	uniform	no unit	J3/mass of full system (dry)
J3m_v	*0.39*	*0.43*	uniform	no unit	J3/mass of entry vehicle
J12_sv	0.77	0.84	uniform	no unit	J1/J3 or J2/J3 of full system (dry)
J12_v	0.76	*0.83*	uniform	no unit	J1/J3 or J2/J3 of entry vehicle
Theta_1_sv	*0.5*		constant	deg	Angle between J3 axis of full system& spin table (z) axis
Theta_1_v	1.7		constant	deg	Angle between J3 axis of entry vehicle& spin table (z) axis
Theta_2_sv	o	0.15	normal	deg	Angle from spin table (z) axis to CS geometic (z) axis
Theta_2_v	*o*	*0.05*	normal	deg	Angle from spin table (z) axis to EV geometric (z) axis
Theta_3_v	o	0.01	normal	deg	Angle from EV geometric (z) axis to CS geometric (z) axis
z_s	0.15	*0.17*	uniform	m	C.M. position (Z) of cruise stage (dry)
z_v	0.8	0.84	uniform	m	C.M. position (Z) of entry vehicle
R_sv	o	0.00025	normal	m	Offset from full system (dry) C.M. to balance axis, x-y plane
R_v	o	0.00025	normal	m	Offset from entry vehicle C.M. to balance axis, x-y plane
o_sv	o	0.0005	normal	m	Offset from balance axis to cruise stage (z) axis, x-y plane
o1_v	o	0.0005	normal	m	Offset from balance axis to entry vehicle (z) axis, x-y plane
02_v	o	0.0005	normal	m	Offset from EV gee. (z) axis to CS gee. (z) axis, x-y plane
Pi	110		constant	N	Initial preload of separation spring
w	44		constant	N	Final preload of separation spring
Stroke	*0.06*		constant	m	Stroke of separation spring
Pi_tol	*-5.5*	*5.5*	uniform	N	Tolerance of initial preload
Pf_tol	-2.2	2.2	uniform	N	Tolerance of final preload
Stroke_tol	-0.0005	*0.0005*	uniform	m	Tolerance of stroke
Omg	*2*		constant	rpm	Pre-separation spin
Omg_tol	-0.1	0.1	uniform	rpm	Tolerance of pre-separation spin
Nut	o	*0.5*	uniform	deg	Maximum pre-separation nutation

* function of fill level

M_p_max and **f_max,** Table 1;

3. Compute geometric centers of four tank, based on Ltc and Ztc, Table 1;
4. Perturb geometric centers of four tanks, based on Dtc, Table 1;
5. Compute c.m.'s of four tank, based on Z_p, dR_p, and dZ_p, Table 1;
6. Migrate propellant across opposite tanks, based on **M_m,** Table 1;
7. Compute total propellant mass, c.m., and moment of inertia of four tanks.

The propellant mass properties will be combined with the dry mass properties of the cruise stage.

5.2 Mass Properties of Cruise Stage & Entry Vehicle

Based on the spin balance requirements and the mass properties table, the mass properties of cruise stage and entry vehicle are chosen as follows [1]:

1. Select dry mass of full system (i.e. cruise stage& entry vehicle, no propellant), and mass of entry vehicle, based on M_sv and M_v, Table 1;
2. Select principal moments of inertia ($J_1 \leq J_2 < J_3$) for dry full system and entry vehicle, based on J3m_sv, J3m_v, J12_sv & J12_v, Table 1;
3. Tilt J_3 -axis to spin table axis (direction of tilt, 0° to 360°, uniformly distributed) for full system and entry vehicle, based on theta_1_sv, theta_1_v, Table 1;
4. Tilt spin table axis to geometric (z) axis (direction of tilt, 0° to 360°, uniformly distributed) for full system and entry vehicle, based on theta_2_sv and theta_2_v, Table 1;
5. Tilt entry vehicle geometric (z) axis to cruise stage geometric (z) axis (direction of tilt, 0° to 360°, uniformly distributed), based on theta_3_v, Table 1;
6. Select z-coordinate for dry cruise stage cm. and entry vehicle cm., based on Z_s and Z_V, Table 1, and then derive z-coordinate of full system cm.;
7. Offset c.m.'s of full system and cruise stage in x-y plane, based on R_sv, R_v, O_SV, O1_v, and O2_v, Table 1;
8. Get wet mass properties of full system by adding propellant mass properties computed above;
9. Derive wet mass properties of cruise stage by subtracting entry vehicle mass properties from Step 8.

5.3 Separation Spring Parameters

The separation springs are used to push the cruise stage off the entry vehicle. There are three separation springs, 120° apart along a circle of 0.259 m radius, at the interface of cruise stage and entry vehicle. . In the ADAMS dynamic model, the constraint condition of guided separation springs is simulated.

Based on the current separation spring design, the nominal spring parameters of initial preload, final preload, and stroke are 110 N, 44 N, and 0.06 m respectively, as shown in Figure 2. To avoid an unacceptable entry attitude error due to the separation torque induced by spring force mismatch, a tolerance of +/-5.5 N, +/-2.2 N, and +/-0.0005 m are specified for the initial preload, final preload, and stroke.

To verify this spring design, the spring parameters for each simulation were selected randomly within their tolerances, as shown by **Pi, Pf, Stroke,** Pi_tol, Pf_tol, and Stroke_tol in Table 1.

5.4 Cable Drag at Two Cutters

There are two electrical cable cutters at the interface of cruise stage and entry vehicle. In spacecraft coordinate system, the approximate (x,y) locations of 1" and 5/8" cutters are (-0.065 m, 0.215 m) and (0.190 m, -0.100 m), respectively. The cable drag will impart a torque during the separation event which may cause an unacceptable entry attitude error.

To cover all possible cases, the cable drag force induced by each cutter is either on or off, randomly combined for each run. The force level remains constant (30, 60, or 90 N) within a separation distance of 0.01676 m.

5.5 Pre-Separation Spacecraft Spin & **Nutation**

Prior to the cruise stage/entry vehicle separation, the spacecraft will be spinning. The specified spin rate is 2 rpm with a tolerance of +/- 0.1 rpm. In the Monte Carlo simulation, the pre-separation spin rate is a random variable with a uniform distribution determined by Omg and Omg_tol in Table 1.

Prior to the separation, the spacecraft will be nutating as well. The nutation angle is defined as the maximum angle

between the spacecraft angular momentum vector and its principal axis. Pre-separation nutation is an important parameter in predicting separation-related pointing errors. Based on the current spec. [1], the parameter of Nut in Table 1 was randomly selected between 0° and 0.5° for each run. The phase of the nutation is chosen randomly from 0° to 360°, uniformly distributed.

Once the pre-separation spin and nutation are selected, they are converted into angular velocities and applied as initial conditions in the ADAMS dynamic model.

6. SIMULATION RESULTS

Five sets of 100 simulations were performed and summarized in Table 2. The CPU time of each run is about 30 seconds on an HP/735 workstation. Figure 1 shows the animation of a typical cruise stage/entry vehicle separation with torque imparted by spring variations and drag force.

Table 2. Summary of Monte Carlo Runs

Run ID	No. of Rum	Spring Variations	Drag (N)	Comments
cs_d Ko_ Doo	100	No	0	<- ideal sep.
cs_dK1_Doo	100	Yes	o	
cs_dK1_D30	100	Yes	30	
cs_dK1_D60	100	Yes	60	
cs_dK1_D90	100	Yes	90	

The uncertainty limits of model parameter dispersions over each 100 Monte Carlo Runs are listed in Table 3. Note that 2000 simulations per set will be performed in the final verification separation analysis.

The results of separation velocity, clearance loss, and entry vehicle angle of attack are presented in terms of their statistical bounds: minimum, maximum, mean+/-3sigma. Due to the sample size of 100, mean+/-3sigma is actually estimated by mean+/-3.65sigma to achieve 99% confidence [4>].

6.1 Separation Velocity

In the simulation, the separation velocity is computed as the relative velocity between the cruise stage cm. and entry vehicle cm. after separation. Figure 3 illustrates the time history of separation velocity, which is based on an ideal separation (no spring mismatch, no drag, 19.8% fill level, cruise stage mass= 239 kg, entry vehicle rnass=491 kg). As indicated by the figure, the separation time is about 0.25 sec.

Figure 4 summarizes the statistical bounds of separation velocity vs. drag force levels. Within the range of drag force assumed, it is clear that the separation velocity requirement of 0.27 m/see is easily satisfied with 99% confidence, as indicated by the mean-3sigrna curve.

6.2 Clearance Loss

During the separation simulation, the radial clearance reduction is tracked by viewing the entry vehicle trajectory from the cruise stage reference, i.e. the relative radial distance from the symmetry axis of the cruise stage to the top geometric center of the entry vehicle. The radial clearance reductions are plotted as functions of the separation distance in Figure 5. The radial clearance reduction profiles envelope the radial motion of the entry vehicle relative to the cruise stage.

Two critical clearances between the entry vehicle and cruise stage are at the cruise stage ring and the propellant tanks. To assess these clearances, the minimum clearance profiles required to avoid any possible contact with the cruise stage ring and tanks are computed and plotted in Figure 5. As compared to the radial clearance reduction profiles, gigantic margins are shown due to the entry vehicle cone angle. As a result, there is no contact during and after the cruise separation event. The hardware clearance between the cruise stage and entry vehicle should therefore be designed to launch vibration environment.

6.3 Entry Vehicle Angle of Attack

To compute the maximum angle of attack of the entry vehicle at at mosphenc entry, θ_{NAV} =1° and θ_{AIM} =1.5° are substituted in equation (1) based on the requirements on other subsystems [1]. θ_{SEP} and μ are obtained from the ADAMS simulation. v is computed directly *from the* mass properties of the entry vehicle, RSS'd with a 10 wobble angle due to heatshield asymmetry.

The entry attitude error results are compared to the requirement of 7° in Figure 6. It is seen that the requirement will be satisfied if the cable drag is below approximately 18 N.

Table 3. Model Parameters for Monte Carlo Simulation of MPF Cruise Separation

Variable	Range over 100 samples Min.	Max.	Units	Description
PLi_1	104.5537	115.4397	N	Initial preload in separation spring (1)
PLi_2	104.5061	115.3024	N	Initial preload in separation spring (2)
PLi_3	104.5097	115.4564	N	Initial preload in separation spring (3)
PLf_1	41.8132	46.1961	N	Final preload in separation spring (1)
PLf_2	41.8082	46.1665	N	Final preload in separation spring (2)
PLf_3	41.8017	46.1253	N	Final preload in separation spring (3)
Stroke_1	0.0595	0.0605	m	Stroke of separation spring (1)
Stroke_2	0.0595	0.0605	m	Stroke of separation spring (2)
Stroke-3	0.0595	0.0605	m	Stroke of separation spring (3)
Rate_1	986.5521	1228.642	N/m	Rate of separation spring (1)
Rate_2	975.8055	1205-2.57	N / m	Rate of separation spring (2)
Rate_3	981.3414	1234..376	N / m	Rate of separation spring (3)
Drag_1	0	0,30,60,90	N	Drag force of 1" cutter
Drag_2	0	0,30,60,90	N	Drag force of 5/8" cutter
Spin_rate	1.9	2.0991	RPM	Spin rate of spacecraft at time of separation
Nutation_sv	0.0225	0.4985	deg	Pre-separation nutation
M_v	476.2298	604.2995	kg	Mass of entry vehicle
X_v	-0.0005	0.0002	m	C.M. position (X) of entry vehicle
Y_v	-0.0004	0.0005	m	C.M. position (Y) of *entry* vehicle
Z_v	0.7991	0.8397	m	C.M. position (Z) of entry vehicle
Ixx_v	151.434	200.3262	kg_m^2	Moments of inertia of entry vehicle about C.M.
Iyy_v	148.4147	202.0408	kg_m^2	Moments of inertia of entry vehicle about C.M.
Izz_v	192.1222	251.2001	kg_m^2	Moments of inertia of entry vehicle about C.M.
Ixy_v	-4.1871	6.5117	kg_m^2	Moments of inertia of entry vehicle about C.M.
Ixz_v	-1.6053	1.568	kg_m^2	Moments of inertia of entry vehicle about C.M.
Iyz_v	-1.575	1.6048	kg_m^2	Moments of inertia of *entry vehicle* about C.M.
Wobble_v	1.6667	1.731	deg	Wobble angle of entry vehicle
M_s_dry	180.9381	243.7685	kg	Mass of cruise stage (dry)
X_s_dry	-0.0012	0.0019	m	C.M. position (X) of cruise stage (dry)
Y_s_dry	-0.0015	0.0014	m	C.M. position (Y) of cruise stage (dry)
Z_s_dry	0.1501	0.17	m	C.M. position (Z) of cruise stage (dry)
Ixx_s_dry	84.9207	157.2949	kg_m^2	Moments of inertia of cruise stage (dry) about C.M.
Iyy_s_dry	88.1902	157.3904	kg_m^2	Moments of inertia of cruise stage (dry) about C.M.
Izz_s_dry	189.4239	266.8364	kg_m^2	Moments of inertia of cruise stage (dry) about C.M.
Ixy_s_dry	-13.4678	13.8901	kg_m^2	Moments of inertia of cruise stage (dry) about C.M.
Ixz_s_dry	-2.1273	2.7108	kg_m^2	Moments of inertia of cruise stage (dry) about C.M.
Iyz_s_dry	-2.1384	2.2771	kg_m^2	Moments of inertia of cruise stage (dry) about C.M.
Fill_level	0.0022	54.3817	%	Propellant tank percent fill level
Prop_mass	0.0034	83.7931	kg	Propellant mass at time of separation
M_s	184.7807	320.6238	kg	Mass of cruise stage (wet)
X_s	-0.0068	0.0064	m	C.M. position (X) of cruise stage (wet)
Y_s	-0.0058	0.0066	m	C.M. position (Y) of cruise stage (wet)
Z_s	0.1516	0.1968	m	C.M. position (Z) of cruise stage (wet)
Ixx_s	98.296	191.9678	kg_m^2	Moments of inertia of cruise stage (wet) about C.M.
Iyy_s	100.4333	199.8729	kg_m^2	Moments of inertia of cruise stage (wet) about C.M.
Izz_s	194.1567	350.9481	kg_m^2	Moments of inertia of cruise stage (wet) about C.M.
Ixy_s	-13.536	13.767	kg_m^2	Moments of inertia of cruise stage (wet) about C.M.
Ixz_s	-2.1737	2.69	kg_m^2	Moments of inertia of cruise stage (wet) about C.M.
Iyz_s	-2.2472	2.51	kg_m^2	Moments of inertia of cruise stage (wet) about C.M.
x_sv	-0.0021	0.0018	m	C.M. position (X) of cruise stage+ entry vehicle (wet)
Y_sv	-0.002	0.0019	m	C.M. position (Y) of cruise stage + entry vehicle (wet)
z_sv	0.5906	0.6485	m	C.M. position (Z) of cruise stage + entry vehicle (wet)

Figure 2. Load-Deflection Curve of Cruise Separation Spring

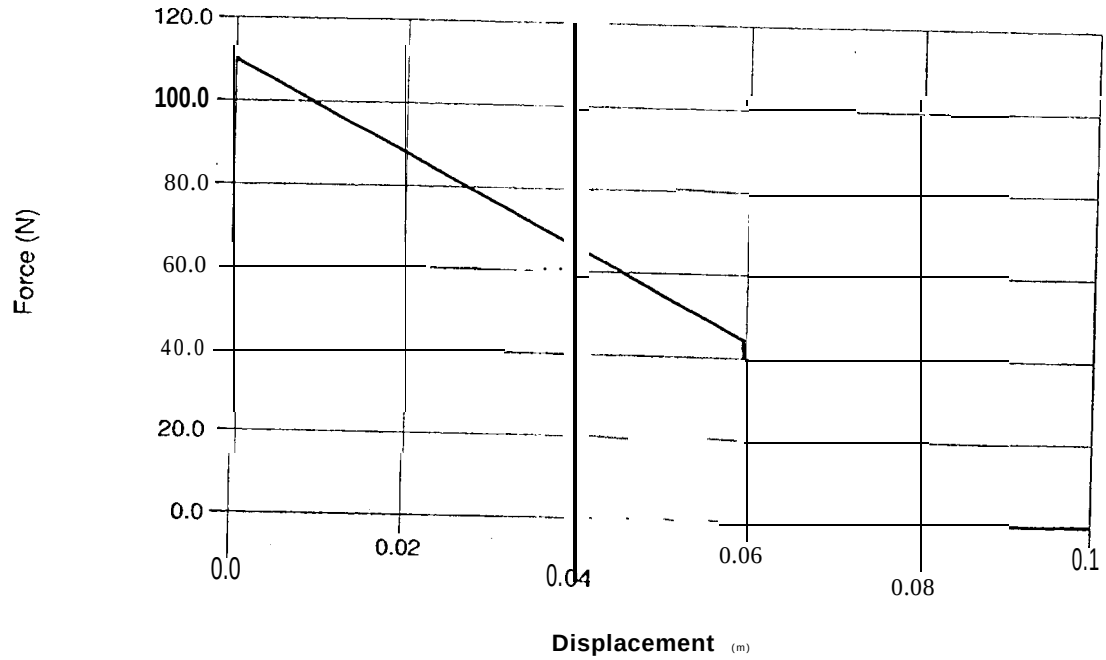

Figure 3. Time History of Cruise Separation Velocity

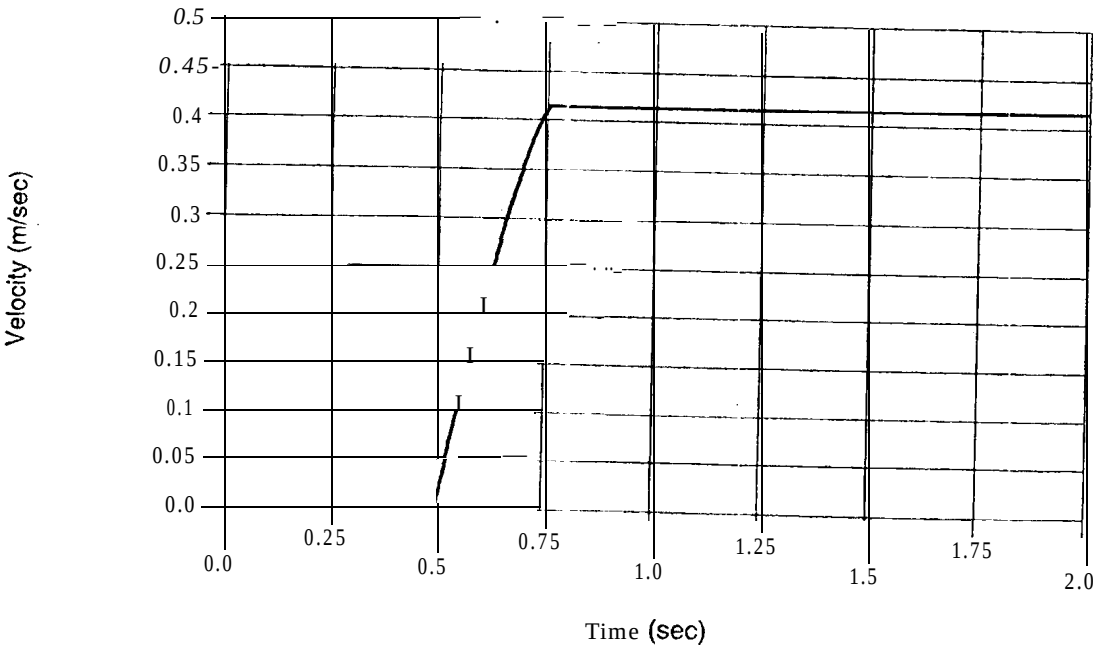

Figure 4. Separation Velocity vs. Cable Drag Force

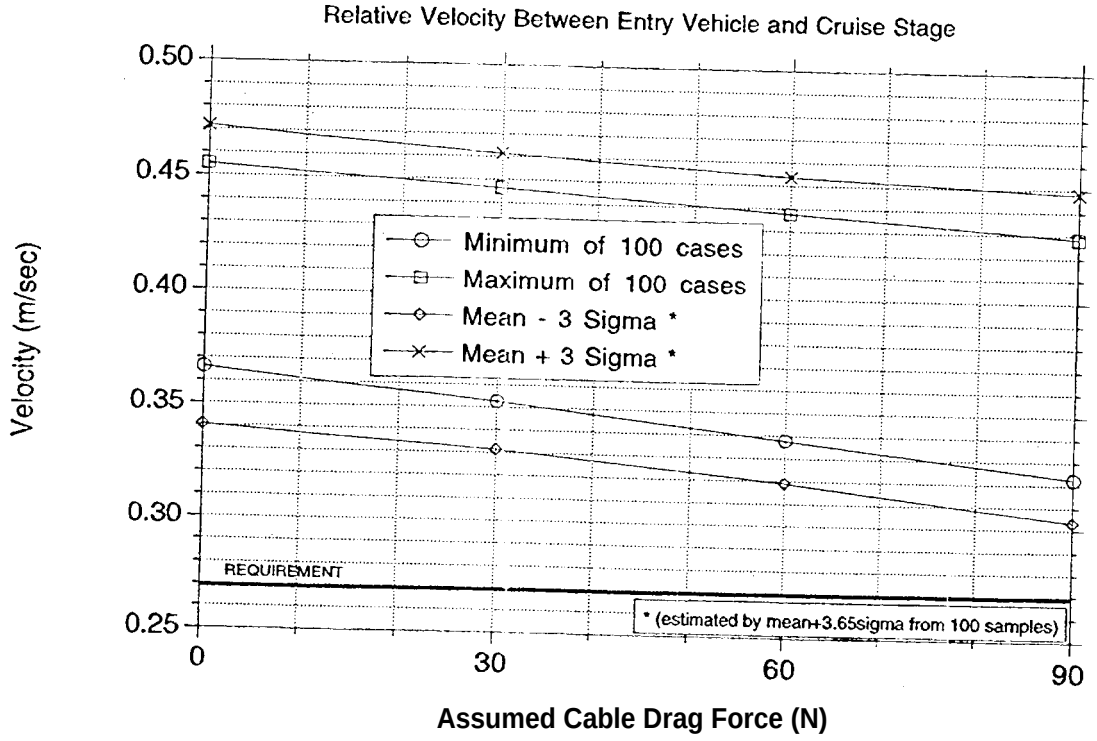

Figure 5. Radial Clearance Reduction vs. Separation Distance

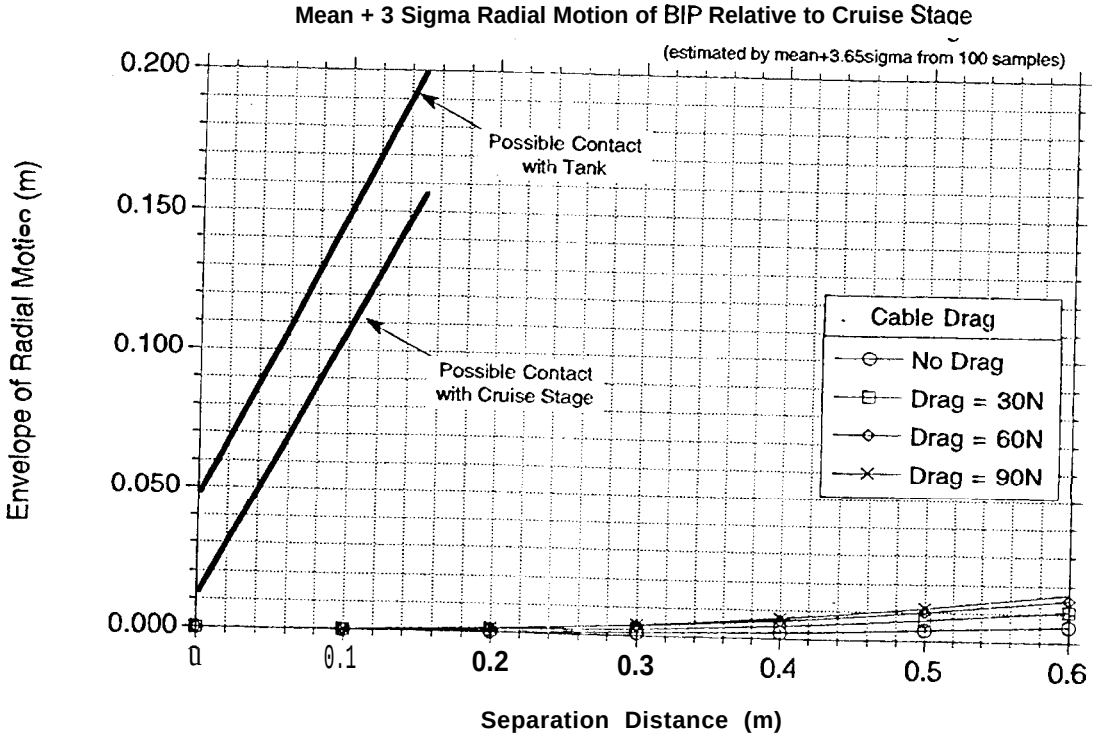

Figure 6. Entry Vehicle Angle of Attack vs. Cable Drag Force

Maximum Angle of Attack at Entry (Includes All Sources)

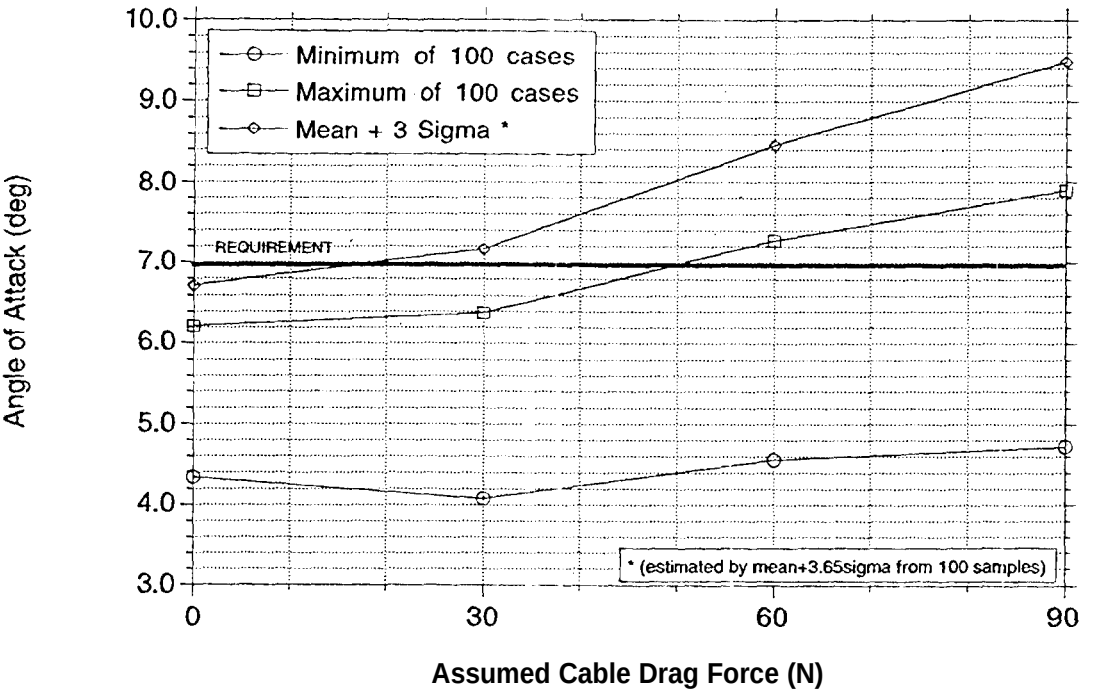

Figure 7. Rotation of H_{EV} vs. Cable Drag Force

Due to Separation Torques Imparted by Spring Variations& Drag

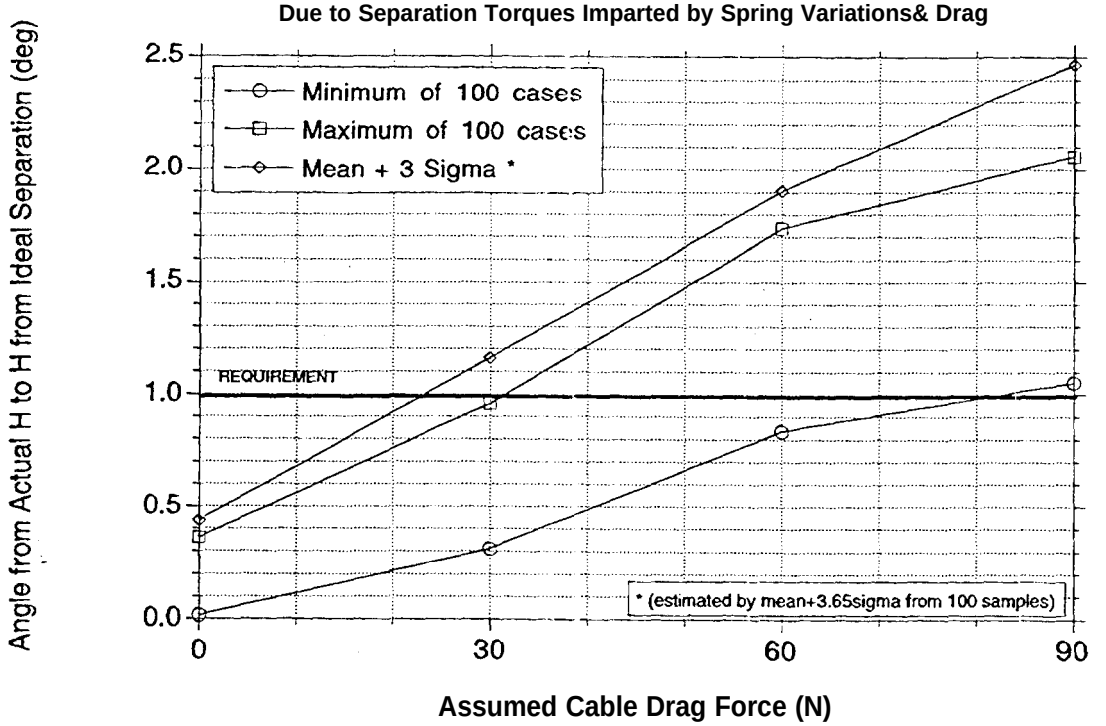

6.4 Entry Attitude Error from Separation Torque

A torque can be imparted between the cruise stage and entry vehicle by a small force differential between the separation springs and by the drag at two cable cutters. This separation torque changes the post-separation angular momentum vector of the entry vehicle, H_{EV}, and can increase the entry attitude error.

The effect of the separation torque on the entry attitude error, is examined by computing the rotation angle of H_{EV} from an ideal separation, and comparing this best-case rotation to the corresponding rotation of H_{EV} with spring variations and cable drag included during the Monte 'Carlo simulation, as summarized in Table 2.

The results are plotted in Figure 7. For the no-drag case, the mean+ 3sigma value of the rotation angle of H_{EV} due to spring parameter dispersions is less than 0.5°. The separation springs were designed to meet this 0.5° requirement. Including both spring variations and cable cutter drag, the rotation of H_{EV} is less than 10 if the cable drag is below approximately 23 N.

7. CONCLUS1ONS

Using the Monte Carlo simulation technique, the separation analysis described above takes into "account the uncertainty of all pertinent design parameters. The analysis predicts the statistical bounds of separation velocity, entry vehicle angle of attack, and a subset of critical clearances with 99% confidence. The Mars Pathfinder cruise separation hardware design is then verified based on these statistical bounds.

The results demonstrate that the current design satisfies the separation requirements, provided drag forces in the cable cutter barrel are less than approximately 18 N per cutter. Therefore, the drag from' the cable cutters must be minimized in order to achieve a successful separation. The actual drag force value should be characterized by tests.

As the flight system continues to develop, it is important to assure that the uncertainty limits of model parameters, listed in Table 3, are not exceeded. However, the cruise separation analysis should be repeated when the entry error budget is changed.

8. ACKNOWLEDGMENT

The work described herein was conducted by the Jet Propulsion Laboratory, California Institute of Technology, under contract with National Aeronautics and Space Administration.

9. REFERENCES

[1] "Mars Pathfinder Project Flight System Requirements and Verification, PF-300-2.0, Rev. A," JPL D-10903, August, 1994, Jet Propulsion Laboratory, California Institute of Technology, Pasadena, California.

[2] Probability and Statistical Inference for Scientists and Engineers, Isaac N. Gibra, Prentice-Hall, Inc., Englewood Cliffs, New Jersey.

[3] "ADAMS/Solver Reference Manual (Version 8.0) and ADAMS/View Reference Manual (Version 8.0)," November 15, 1994, Mechanical Dynamics, Inc., Ann Arbor, Michigan.

[4] Alfredo H-S. Ang and Wilson H. Tong, "Probability Concepts in Engineering Planning and Design, Volume 1: Basic Principles, " John Wiley& Sons, Inc., New York,

[5] Julius S. Bendat and Allan G. Piersol, "Engineering Applications of Correlation and Spectral Analysis," John Wiley & Sons, Inc., New York.